Pergamon

Cement and Concrete Research 31 (2001) 1847–1858

CEMENT AND CONCRETE RESEARCH

The utility of a bimolecular expression to describe the heat generation and temperatures in curing Class HP concrete

Gary S. Wojcik[a,*], Joel L. Plawsky[b], David R. Fitzjarrald[a]

[a]*Atmospheric Sciences Research Center, University at Albany, State University of New York, 251 Fuller Road, Albany, NY 12203-3649, USA*
[b]*Department of Chemical Engineering, Rensselaer Polytechnic Institute, Troy, NY 12180-3590, USA*

Received 3 January 2001; accepted 24 September 2001

Abstract

For several days after concrete is poured, atmospheric conditions influence the hydration reactions of concrete's binder components and so may influence its long-term durability. Accurate concrete temperature and moisture forecasts would help engineers determine an optimal pour time. Some existing curing concrete models include complicated chemistry and/or microstructure development parameterizations or do not allow for mix design changes. A bimolecular heat generation expression that is simple but sufficiently detailed to account for mix design changes was improved for Class HP concrete. Analysis of published calorimetry data and those determined in this study indicated that a second-order formulation adequately describes the heat generation. Class HP binder has an activation energy of $\sim$35 kJ mol^{-1}. After 72 h, Class HP pastes evolved 250–280 kJ kg^{-1}. A method to account for the effect of retarders on Stage II length and Stage III hydration rates was developed. A curing concrete bridge model with the bimolecular expression predicted concrete temperatures to within 2 °C of observed temperatures and reasonable 72-h hydration fractions ($\sim$0.6). © 2001 Elsevier Science Ltd. All rights reserved.

Keywords: Hydration; Calorimetry; High-performance concrete; Blended cement; Fresh concrete

1. Introduction

Ambient atmospheric conditions influence the thermal and moisture state of freshly poured, curing concrete. The long-term durability and strength of the resulting concrete mass may be compromised by excessive concrete temperatures and temperature gradients or insufficient moisture during the first few days after the concrete is placed [1–4]. These durability problems contributed to the need to replace an average of 12 bridge decks per year at an annual cost of US$20 million in New York State from 1995 to 1999 (K. McCarty, 1999, personal communication).

We developed a model to determine how ambient atmospheric conditions influence the thermal and moisture state of curing concrete on bridge decks during the first few days after placement. The model is simple enough for use in a field setting so the field engineer may determine an optimal time to pour based on weather forecasts, and is flexible enough to accurately account for the heat and mass transfer which occur in any atmospheric conditions. In addition, the model's heat generation expression, the focus of this paper, is simple and flexible enough to be applied if a field engineer decides to augment the water-mass-to-binder-mass ratio (w/b) of the concrete mix.

Proper boundary conditions for the model were determined from four field campaigns in which the energy balances of four curing concrete bridge decks in eastern and central New York were estimated from atmospheric and bridge environment measurements [5]. At the top surfaces, heat was transferred by evaporation, convection, radiation and runoff spray water. Because the magnitude of each transfer term varied depending on the atmospheric conditions, all terms must be included as boundary conditions in a realistic model of curing concrete bridge decks. From these energy balances, heat and mass exchange coefficients for convection and evaporation were found to be a function of an easily determined atmospheric stability parameter. Heat transfer at the bottom of the bridge was less than 30% of that at the top and was dominated by conduction through steel support beams, which produced large concrete temperature gradients above the beams.

* Corresponding author. Tel.: +1-518-437-8726; fax: +1-518-437-8758.
E-mail address: gary@asrc.cestm.albany.edu (G.S. Wojcik).

PII: S0008-8846(01)00692-5

This paper describes the development of the hydration heat generation expression for the curing concrete model. For its bridge decks, New York State Department of Transportation (NYSDOT) now specifies the use of Class HP concrete whose binder component is composed of 74% cement, 20% flyash and 6% microsilica by weight, a variation of Class H concrete which uses 85% cement and 15% flyash. The NYSDOT has determined the physical properties of Class HP concrete such as a 28-day strength of 6350 psi [6]. The thermal conductivity, density, specific heat capacity and the 24-h hydration heat of Class HP concrete are 2.7–3.0 W m^{-1} K^{-1}, 2230 kg m^{-3} and 1380 J kg^{-1} K^{-1} and $\sim$190 kJ kg^{-1}, respectively [5]. However, no detailed rate information about the hydration reactions of Class HP concrete is available.

The NYSDOT also requires the use of an acceptable set-retarding/water-reducing admixture. For the 1998 and 1999 bridges, the set-retarding/water-reducing admixtures used were hydroxycarboxylic acids: W.R. Grace's Daratard 17 and Sika's Plastiment, respectively. We do not know what types of retarders were used for the 1995 or the 1996 bridges. By adsorbing onto the hydration products, these retarders limit the movement of water toward the unhydrated binder [1] and slow the hydration reactions. Retarders have been studied extensively [7,8] but because of the complexity of the interaction of retarders with different binder compositions, no detailed mechanisms that describe their effect on the hydration reactions are available. In a technical bulletin for Daratard 17, Grace provides information of dosage rate versus set time for several concrete temperatures. For example, for concrete at 21 °C and a dosage rate of 4 oz (100 lb binder)$^{-1}$, the set delay (increase in the length of Stage II) is about 4 h. However, manufacturers generally recommend that the retarders be tested with samples of the exact materials to be used in the concrete. NYSDOT has not conducted any experiments to determine the action of these retarders. We have conducted experiments to determine the effect of the retarders on the heat evolution of the hydrating Class HP binder.

To meet the intended purposes of our model, the heat generation expression for Class HP concrete must be simple but also flexible enough to allow for mix design changes. Some existing hydration parameterizations contain detailed chemical reactions for several compounds consumed or formed during the hydration process [9,10]. Such parameterizations are too complex for our stated goals.

Another common approach to calculating the heat generation rate is the chemoplasticity approach, which was first suggested by Acker et al. [11], and has been described in the thermodynamic framework of a reactive, porous media by Ulm and Coussy [12,13] and Ulm et al. [14]. In the chemoplasticity approach, the heat generation rate at any given time is dependent upon temperature and the fraction of the binder that has hydrated up to that point, α. To predict the heat generation for a particular mix under any conditions, all that is needed is temperature and heat data from one calorimetry experiment for that mix. While very simple, this approach cannot handle changes in mix design (since a different calorimetry experiment would be needed)—an important feature of our expression.

A bimolecular parameterization with published reaction rate constants to predict heat generation rates was used in a finite element model of curing concrete pavements [15] and bridge decks [16]. Concrete temperature predictions were within about ± 2–5 °C of field observations. The model also predicted the location of maximum temperatures near the bottom of the deck and the localized temperature minima above the support beams (Fig. 1a), as seen in the observed data. However, subsequent analysis revealed that the expression produced too much heat over a longer period than indicated by the observations and could not simulate any part of Stage II, which was extended by the addition of retarders into the concrete mix (Fig. 1b).

To formulate the heat generation expression for Class HP concrete, we used a bimolecular formulation in which the hydration rate of the binder components, r_B (mol_B m^{-3} s^{-1}), is a function of the binder components and water concentrations:

$$r_B = -kR^m B^n \quad (1)$$

where k is the effective rate constant (m^3 mol_R^{-1} s^{-1}) and is dependent on temperature, given with an Arrhenius

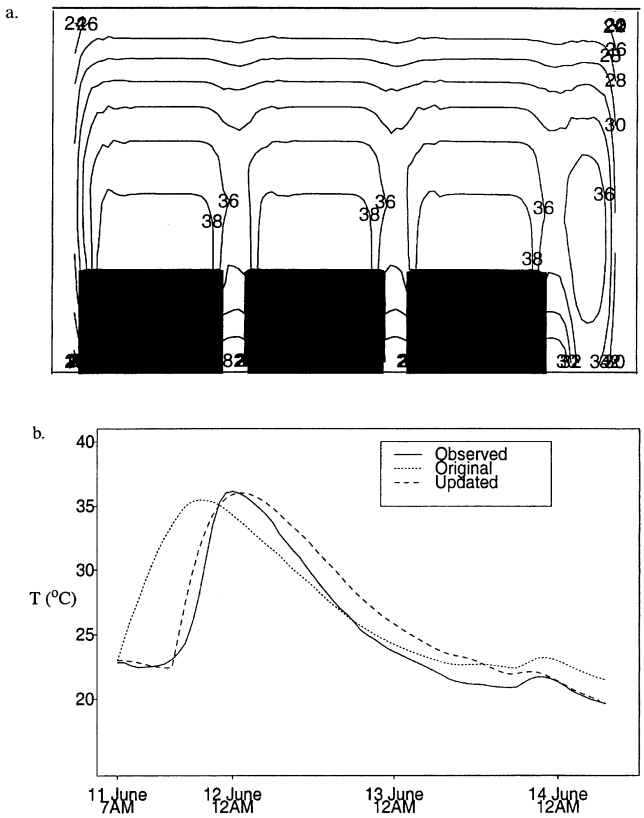

Fig. 1. (a) Predicted concrete temperatures for a cross-section of a curing concrete bridge deck in Saratoga, NY, in June 1998. The thicker concrete areas are supported from below by steel support beams. (b) Observed and predicted temperatures near the bottom of the concrete slab.

term $A\exp(-E_a/R^*T_{sys})$: where A is the pre-exponential factor, E_a is the activation energy (J mol^{-1}), R^* is the universal gas constant (J mol^{-1} K^{-1}) and T_{sys} is the reaction temperature in Kelvin; R and B are the available water (mol$_R$ m^{-3}) and binder (mol$_B$ m^{-3}) concentrations in the concrete, respectively; and m and n are exponents providing the overall order of the reaction, $m+n$. The cement, flyash and microsilica are lumped into B as we treat them as a single material.

In our model, we explicitly compute the binder and available water concentrations:

$$\frac{dB}{dt} = -A\exp\left(-\frac{E_a}{R^*T_{sys}}\right)R^mB^n \quad (2)$$

$$\frac{dR}{dt} = \eta\frac{dB}{dt} \quad (3)$$

where η is the number of moles of water consumed per mole of binder consumed and includes the chemically combined water and that adsorbed on the hydration products [17]. η in relation to R may also be interpreted as an indication of the decrease in the water concentration in the capillary pores before they become segmented [18]. See Wojcik [19] for a more complete discussion of η, which can range from 3 to 12 [1,9,18,20,21].

A heat generation expression can be formulated from Eq. (1):

$$\frac{dq}{dt} = k(-\Delta H)R^mB^n \quad (4)$$

where dq/dt (J m^{-3} s^{-1}) is the time derivative of hydration heat per unit volume of concrete and $-\Delta H$ (J mol$_B^{-1}$) is the specific hydration heat of Class HP concrete.

A bimolecular formulation for the hydration reactions is plausible because the hydration reactions are similar to the bimolecular nucleophilic substitution reactions in the sol–gel process for producing ceramics. Since the sol–gel process is first order in both reactant concentrations, we assumed $m=1$ in Eqs. (1), (2) and (4) [22,23]. We recognize that the hydration process in concrete or cement paste is controlled by the chemical reactions during the early stages of hydration (up to $\alpha\sim0.5$), but after this time may be limited by the transport of water through the bulk material and the hydration products themselves [17,23]. Because we explicitly compute the binder and available water concentrations, the predicted reaction rates will gradually decrease as the concentrations of both these variables decline, mimicking the transition from a kinetically controlled state to a diffusion-controlled state.

Is the simplest bimolecular parameterization ($m=n=1$) reasonable? Support for assuming $n=1$ in Eqs. (1), (2) and (4) can be found by creating a dimensionless expression from Eq. (2) and by comparing its solutions with calorimetry data (Fig. 2). We used the hydration heat as an indication of the extent of the hydration reactions as is commonly done

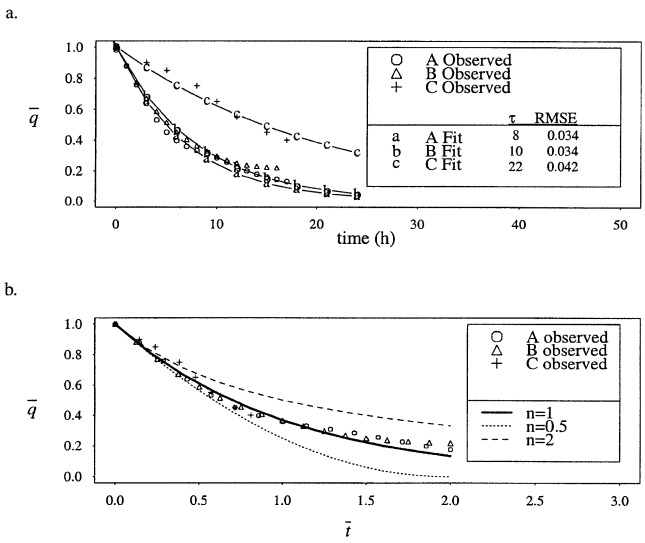

Fig. 2. (a) Time series plots of observed and fitted dimensionless heat evolution rates ($\bar{q}$, heat evolution rates scaled by the peak rate) beginning at the time of the peak rate. Sample A is for a paste with CCRL cement 133 at 25 °C for w/b = 0.3; B is for a paste with CCRL cement 133 at 25 °C for w/b = 0.45; and C is for a paste of 80% cement and 20% flyash at 20.5 °C for w/b = 0.5. CCRL cement 133 contains 70% C_3S, 13% C_2S, 8% C_3A, 8% C_4A and 5.4% gypsum by volume. The τ (h) indicated in the legend is the characteristic time of the evolution rates determined by minimizing the RMSE between the observed and exponential fitted times series. (b) Similarity plots of dimensionless heat evolution rates vs. dimensionless time, $\bar{t}$. Values for n indicate powers for the binder concentration in Eq. (1).

[24,25] (see Section 2.2). With $m=1$ and if $n=1$, Eq. (2) can be recast and solved to yield a simple exponential in dimensionless terms (Eq. (5)):

$$\bar{q} = \exp(-\bar{t}) \quad (5)$$

where (Eq. (6))

$$\bar{q} = \frac{q}{q_0} \quad (6)$$

where (Eq. (7))

$$\bar{t} = \frac{t}{\tau} \quad (7)$$

and where (Eq. (8))

$$\tau = \frac{1}{kR} \quad (8)$$

The peak heat generation rate is given by q_0 and τ is the length of time (h) after the time of the peak rate (t_0) at which q drops to $1/e$ of q_0.

If $n\neq1$, the dimensionless expression is (Eq. (9)):

$$\bar{q} = \{1-[(1-n)\bar{t}]\}^{\frac{1}{1-n}} \quad (9)$$

To make these dimensionless forms, we have assumed that k and R show little variation with time from the time of the peak rate to about 20 h after the peak. To validate these assumptions, we used calorimetry data for the hydration of

the Cement and Concrete Reference Laboratory (CCRL) cement 133 at a temperature of 25 °C and w/b = 0.45 [26]. For these conditions, k varied < 1% over the course of the reaction due to small changes in the reaction temperature. By using the hydration heat as an indication of the extent of the reaction and by assuming $\eta \sim 7$ (implying that 6 mol of water are chemically combined per mole of binder reacted and that the gel porosity is 19% for a binder system with silica fume [1,20,21,27]) in Eq. (3), we estimate that R decreased by ~35% over this period for this CCRL cement. Though R is not constant, these changes in R are tolerable for our purposes as will be seen in the following.

An exponential parameterization ($n = 1$) of heat generation after the time of the peak rate predicts the observed heat generation rates from the time of the peak up to about 20 h after the peak rate to within 12% as given by calorimetry data for CCRL cement 133 at 25 °C for w/b = 0.3 and 0.45 [26] and by Meland [28] for a sample of 80% Type I cement and 20% flyash cured at 20.5 °C in a conduction calorimeter (Fig. 2). The characteristic time τ of the 25 °C reactions was 7–8 h, while that for the 20.5 °C reactions was about 22 h, as determined by fitting an exponential curve to the observed data and minimizing the root mean square error (RMSE) of heat generation rates given by each value of τ selected. Because this calorimetry data can be fit with an exponential expression, our assumption that $n = 1$ is reasonable. Note that since the bimolecular and exponential expressions indicate a decreasing heat generation rate with time from the peak rate, the overall integrated heat will be lower than observed. By beginning the calculation of the heat generation rates by at most 3 h earlier, the parameterization does predict the observed integrated heat.

Our formulation for Class HP heat generation can be written as follows:

$$\frac{dq}{dt} = A\exp\left(-\frac{E_a}{R^* T_{sys}}\right) \times (-\Delta H) R_0^{n+m} \left\{(1-\alpha)^n \left(\frac{R_0}{B_0} - \alpha\eta\right)^m\right\} \quad (10)$$

where R_0 and B_0 are the initial water and binder concentrations in the concrete. Eq. (10) expresses the heat generation rate as a function of α and temperature, as is done with the chemoplasticity approach. Our formulation, however, is also dependent on the water and binder concentrations (through α, η, R_0 and B_0). If a field engineer decides to change the w/b of the concrete mix, our formulation can be implemented.

Because of the large number of reactions (both from the cement and the flyash and microsilica) that occur during the hydration, E_a in the rate constant expression should be considered an "apparent" activation energy [9,24]. E_a for pozzolan materials (microsilica and flyash in the case of Class HP concrete) is much larger (~ 80 kJ mol^{-1} [29,30]) than that for cement (35–41 kJ mol^{-1} [9] and 32.0–45.7 kJ mol^{-1} [24]). Moreover, while it is often assumed that E_a is constant throughout the hydration process, Kada-Benameur et al. [24] suggest that this is true only up to a hydration fraction of $\alpha = 0.5$. Beyond $\alpha = 0.5$, the hydration process increasingly becomes controlled by diffusion of water through the hydration products to the unreacted binder as opposed to being controlled by the chemical reactions. During such stages of the hydration process, the Arrhenius expression may not be valid. However, we will show that our model formulation can simulate the transition from the reaction rate-controlled stage to the mass transfer rate-controlled stage of the concrete hydration process.

With different compositions and E_a, the binder components react at different times and under different conditions. For example, microsilica reacts when $Ca(OH)_2$ produced by the hydrating cement saturates the pore solutions and up to 50% of the silica may react within 24 h [31]. For Class F flyash, the reactions may not begin until a week or more after mixing when the pore solution attains a pH = 13.2 or greater [32]. With a hydration heat of 780 kJ kg^{-1} [33], the microsilica may contribute more heat evolution during the critical first day of curing than would be the case with no cement (~ 420 kJ kg^{-1}) replacement [34–36].

To refine the bimolecular heat generation parameterization first implemented by Kapila et al. [15] and Plawsky and Kapila [16], we performed laboratory calorimetry experiments. Because we were not able to determine directly the mass changes of the binder components during the hydration reactions, we used the hydration heat as an indication of the extent of the hydration reactions. Binder components taken from the stock used at bridges in 1998 and 1999 [5] were mixed with excess water to find appropriate rate constants and the order of the Class HP hydration reactions. We examined the effect of Daratard 17 and Plastiment on the heat evolution by comparing samples with retarder to those without retarder. In addition, we modeled several of our calorimetry experiments to determine appropriate chemistry parameters in Eq. (2). We also modeled the heat generation and temperature development of a curing concrete bridge deck to further validate our approach. To determine a bulk bimolecular expression in which the cement, flyash and microsilica are lumped together as one species, we necessarily had to avoid the specific details of the reactions of the individual species as discussed above.

In the following, the methodology used to determine the components of the heat generation expression, including the overall hydration heat, reaction order and rate parameters such E_a and A, is described in Section 2. The results of the laboratory experiments along with a comparison of these results to other published values are discussed in Section 3. Our conclusions and their implications are presented in Section 4.

2. Methods

2.1. Determining $-\Delta H$

To determine $-\Delta H$ in Eq. (4), calorimetry experiments were performed with samples of cement, flyash and microsilica taken from the stock used for the concrete at the 1998 and 1999 bridges we studied in the field (Table 1) [5]. $-\Delta H$ is the amount of heat that is evolved when all the binder has hydrated. In our experiments, we could only accurately determine heat evolution up to $\sim$72 h when the decreasing heat evolution rate could no longer be detected with our calorimeter. To estimate the ultimate value of $-\Delta H$, we assumed that about 65% of the binder hydrates by 72 h [37,38] and extrapolated this value to the value at complete hydration.

Binder pastes were produced in the laboratory with w/b of 0.37 and 0.38 and with air entrainers and retarders as specified by NYSDOT for Class HP concrete (Tables 1 and 2). The calorimetry setup consisted of a reaction chamber ($\sim$535 ml) created out of 3 in. diameter copper tubing and end caps, placed inside a water-filled 2-l Dewar flask, all enclosed in a R11 foamboard box packed with R38 fiberglass insulation (Fig. 3). With copper-constantan thermocouples and a Campbell Scientific 23X datalogger, concrete, water and insulation temperatures at 5-s intervals were measured as the sample hydrated for at least 72 h. The data were saved as 5-min averages. For these experiments, no attempt was made to maintain the hydration temperature at a constant value.

Each sample's hourly hydration heat generation rate, Q_{tot} (J s^{-1}), was determined from the paste and water temperature changes and by estimating the heat capacity of the calorimeter and the heat loss from the calorimeter (Eq. (11)):

$$Q_{tot} = C_L(T_{fw}-T_{ins}) + c_{cp}\left(\frac{T_{cp}^{t+l}-T_{cp}^{t}}{\Delta t}\right) + c_{fw}\left(\frac{T_{fw}^{t+l}-T_{fw}^{t}}{\Delta t}\right) \quad (11)$$

where T_{ins} is the insulation temperature (K) and T_{fw} is the temperature inside the flask (K); T_{cp} is the temperature of the paste sample (K); c_{fw} is the heat capacity of the flask–water system (J K^{-1}); c_{cp} is the heat capacity of the reaction chamber and paste sample (J K^{-1}); C_L is the rate of heat transfer per hour from the flask per unit temperature difference between the flask and the surrounding insulation (W K^{-1}), i.e., the thermal resistance of the system; t is time; and $\Delta t = 3600$ s is the time difference between averaged temperature data.

Table 1
Information about the concrete mixes from which were taken the binder solids used in the calorimetry experiments

	1998	1999
Cement type	Type II	Type I/II
Flyash type	Class F (low calcium)	Class F (low calcium)
w/b	0.37	0.38
Retarder [(oz) 100 lb cement solids $^{-1}$]	5 Daratard 17	4 Plastiment
Air entrainer [(oz) 100 lb cement solids $^{-1}$]	5	1.7

Table 2
Information about and results from the variable temperature calorimetry experiments used to determine $-\Delta H$ in Eq. (4)

Experiment	Starting temperature (°C)	Peak temperature (°C)	w/b	Paste mix	AE	RET
98a	22	44	0.37	HP	Y	N
98b	23	38	0.37	HP	Y	N
98c	21	38	0.37	HP	Y	N
98d	23	47	0.37	Type II	Y	N
98e	23	39	0.37	HP	Y	Y
99a	25	43	0.38	HP	Y	N
99b	24	43	0.38	HP	N	N
99c	27	45	0.38	HP	Y	N
99d	27	45	0.38	HP	Y	Y
99e	24	49	0.38	Type I/II	Y	N
99f	24	42	0.38	HP	Y	N
99g	29	46	0.38	H	Y	Y

The binder components were taken from the stock used at the 1998 and 1999 bridges. The "starting temperature" refers to the temperature inside the flask when the reaction chamber was inserted. "Peak temperature" refers to the maximum temperature experienced by each cement paste sample. "AE" and "RET" represent whether air entrainer and retarder were used by "Y" for yes and "N" for no. The "paste mix" indicates the mix of binder solids used in each experiment. "HP" uses cement, flyash and microsilica; "H" uses cement and flyash.

The heat capacity of the calorimeter (flask, water and reaction chamber), c_{tot}, is the result of the addition of two components: $c_{tot} = c_{cp} + c_{fw}$. The difference of c_{tot} and c_{fw} gives c_{cp}. To determine c_{tot} and c_{fw}, two methods were used. First, a known mass of KNO_3, whose heat of dissolution in water at 298 K is 34.89 kJ mol^{-1}, was dissolved in 298 K water. With a prescribed KNO_3 mass, the amount of heat consumed in the dissolution was known and with the

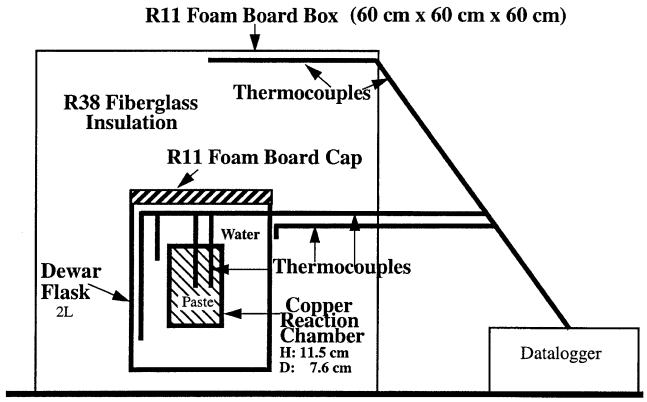

Fig. 3. Schematic diagram of the calorimetry setup for the variable temperature calorimetry experiments used to determine $-\Delta H$. Note that in regard to the reaction chamber, H is the height and D is the diameter.

temperature change of the calorimeter components, c_{tot} and c_{fw} were determined.

The second method to determine c_{tot} and c_{fw} involved heating copper slugs (specific heat capacity of 385.11 J kg^{-1} K^{-1}) to a known temperature and then placing them in the water-filled flask. With the temperature change of copper slugs (the initial copper temperature − the final temperature inside the flask) the amount of heat transferred to the calorimeter was determined. With this heat and the temperature change of the flask and water, c_{tot} and c_{fw} were calculated. The values determined with the copper were within 5% of those determined with the KNO_3, suggesting that the estimated heat capacities were reasonable values.

C_L was found by placing a previously hydrated paste sample inside the water-filled flask at a temperature of 328 K and tracking the temperature inside the flask and in the surrounding insulation as the flask and its contents cooled. With c_{tot} and the temperature changes inside the flask, the rate of heat loss from the flask was determined. Linear regression provided the expression relating heat loss to the temperature difference between the inside of the flask and the surrounding insulation. Heat loss rates were generally <0.05 W K^{-1}.

2.2. Determining k, n, E_a and A

The other parameters in Eq. (2) were determined with constant temperature calorimetry experiments through the method of excess [39]. In practice, for the hydration reactions, the only component of the system that can be used in excess is water. We assumed that the heat generation reactions were first order in R, i.e., $m=1$ in Eq. (2) as is the case with the sol–gel process, and forced the system to be independent of R by using a large excess of water so that R was not a function of time.

To maintain the reaction temperature at a constant value, antifreeze at a fixed temperature was circulated with a Polyscience Model 910 circulator through a copper coil placed inside the flask of the calorimeter. An RZR1 mixer made by Heidolph Instruments (Cinnaminson, NJ) was used continuously to mix the water and binder components in the flask. Temperatures of the antifreeze entering and leaving the flask, the mixture and the insulation were taken every 5 s and saved as 5-min averages. The experiments were allowed to continue uninterrupted for up to 96 h, and were run for w/b = 1.9, 2.4 and 3.5 at temperatures of 20, 30 and 40 °C (Table 3).

To determine the hydration heat, the temperature difference between the antifreeze as it entered and left the flask, the antifreeze heat capacity and flow rate were used. The flow rate was measured with an HGM1-RRP oval gear flowmeter from Venture Measurements (Buffalo, NY). To account for heat transfer to and from the flask from its environment, a steady-state temperature difference of the circulating antifreeze (when the hydration reactions were generating little heat) was determined. This factor was subtracted from the raw antifreeze temperature difference to give the desired hydration heat signal.

Table 3
Information about and results from the excess water experiments performed with the 1999 binder samples

Experiment	Temperature (°C)	w/b	Peak heat generation rate (J kg^{-1} s^{-1})	24-h cumulative heat generation (kJ kg^{-1})	24-h cumulative heat generation uncertainty (%)
E1	20	1.9	1.9	95	10
E2	20	1.9	1.8	95	10
E3	20	2.4	1.8	110	10
E4	20	3.5	1.4	75	20
E5	20	3.5	1.5	80	15
E6	30	1.9	3.1	120	29
E7	30	2.4	3.4	130	24
E8	30	3.5	3.2	140	18
E9	40	1.9	6.4	120	50
E10	40	2.4	7.2	85	65
E11	40	3.5	5.7	120	50

The regression of the natural logarithm of the hydration heat rate with the natural logarithm of B at a given temperature produces a line of slope n and an intercept of k from Eq. (1). A more detailed k with the form of an Arrhenius expression was determined with the regression of the natural logarithm of hydration heat with $1/T$ at a set w/b, which gives a line whose slope is $-E_a/R^*$ with an intercept of $AR_0{}^mB_0{}^n(-\Delta H)$. With values for the other terms in this intercept expression, A was calculated.

We also modeled the temperatures of a variable temperature calorimetry experiment to determine A and to validate our bimolecular formulation. The temperature equation is:

$$\frac{dT_{sys}}{dt} = -N\frac{dB}{dt} + C_L(T_{sys} - T_{env}) \quad (12)$$

where the second term on the right-hand side of Eq. (12) is a source term which accounts for boundary heat transfer; N (K m^3 mol$_B{}^{-1}$ s^{-1}) converts the reacted binder concentration to heat and is equal to $\Delta H^* \cdot \text{vol}/c_{tot}$ where vol is the volume of the flask and $c_{tot} \sim 6000$ J K^{-1} is the heat capacity of the system; T_{sys} is the overall temperature of the calorimeter considering the water and the reaction chamber; and T_{env} is the measured temperature of the insulation surrounding the flask. Eqs. (2) and (3) complete the equations for this simple model.

3. Results

3.1. Variable temperature calorimetry: (−ΔH)

Several calorimetry experiments were performed on the binder solid pastes, with different starting temperatures and components (Table 2). The resulting heat evolution rates exhibited the expected dormant period, rapid heat evolution period and declining heat rate period (Fig. 4). Note that the

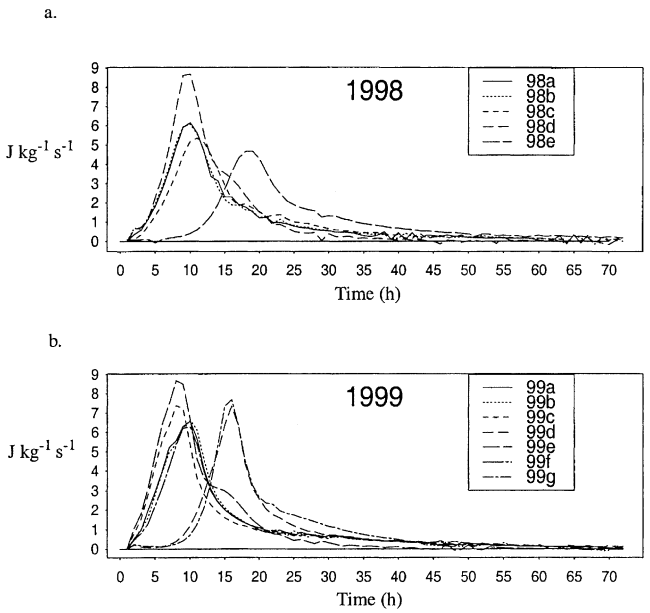

Fig. 4. Heat evolution rates (J kg^{-1} s^{-1}) for Class HP and Class H binder pastes for (a) the 1998 bridge and (b) the 1999 bridge. These rates were determined with the calorimeter as given in Fig. 3. Table 2 provides mix and temperature information about these experiments.

initial surface reactions upon mixing the binder components with water occurred during mixing of the pastes and do not show up on these plots. The dormant period was extended for those samples that contained retarder (Experiments 98e, 99d and 99g). Those samples for which some cement was substituted with microsilica and flyash had lower peak heat generation rates than those samples for which there was no substitution (Experiments 98d and 99e). With more cement, these two samples produced more heat and experienced higher temperatures than the blended samples.

Evolution rates for Experiments 98d and 99e have a secondary peak at 17 h. This secondary peak was due to the appearance of free aluminates within the paste as the gypsum in the mix was exhausted [1], suggesting that our calorimeter setup was sensitive enough to capture features as minor as this secondary peak.

The Type I/II cement from the 1999 samples produced about 3% more heat on average than the Type II cement from the 1998 samples after 72 h–301 kJ kg^{-1} binder solids vs. 292 kJ kg^{-1} (Fig. 5). The 1999 HP samples with no retarder produced up to 9% more heat than those from the 1998 samples (277 vs. 255 kJ kg^{-1}). This difference was most likely the result of higher starting temperatures for the 1999 samples (Table 2) and different binder compositions. The cumulative heat values for the cement and the HP pastes ranged from 250 to 301 kJ kg^{-1} after 72 h, reasonable estimates compared to published 72 h values by Verbeck and Foster [38] (Type II: 200 kJ kg^{-1}; Type I: 260 kJ kg^{-1}) and the Bureau of Reclamation [40] (Type II: 272 kJ kg^{-1}). Therefore, for the 1998 Class HP samples, $-\Delta H = 395$ kJ kg^{-1} and, for the 1999 samples, $-\Delta H = 430$ kJ kg^{-1}, assuming that 65% of the binder was hydrated by 72 h. We do not know the actual hydrated fraction, but expect that it was between 0.5 and 0.75 [37,38], giving an uncertainty in $-\Delta H$ of about $\pm 15\%$.

The two retarders tested produced different features in the hydration reaction. For 98e in which Daratard 17 was used, Stage II was extended from about 2 h for 98a–c with no retarder to about 10 h (a set delay of 8 h). Such set delays are slightly longer than those suggested in the Daratard 17 technical bulletin (about 6 h). The Plastiment in 99d extended Stage II from about 1 h to about 9 h (a set delay of 8 h) in comparison to 99a–c. No manufacturer data on set delays are available for this admixture. The average Stage II hydration rates for these retarders were about 1/10 of the average value during Stage III.

The peak heat evolution rate with the Daratard 17 was reduced from ~ 6 to ~ 5 J kg^{-1} s^{-1}. However, the Plastiment did not significantly affect the Stage III hydration rates in comparison to the Stage III reactions of 99a–c. The total heat evolved by 98e by 72 h was within 1% of that evolved by 98a–c. The heat evolved by 99d was 5% less than that from 99a–c.

To model the reduced hydration rates during Stage II, we make the Stage II reaction rate constant 1/10 of the value of the Stage III rate constant, by reducing A in Eq. (2) by a factor of 10 as indicated by the calorimetry data. After this time, A is increased to the value determined for Stage III (see Section 3.2). The length of Stage II for the 1998 bridge will be determined with the set delay data given in the Daratard 17 technical bulletin and our calorimetry data. We

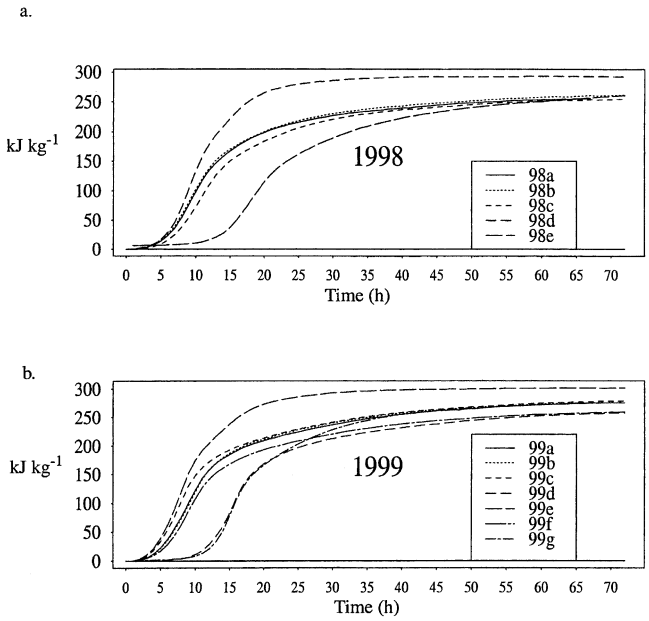

Fig. 5. Cumulative hydration heat evolution (kJ kg^{-1}) for Class HP and Class H binder pastes for (a) the 1998 and (b) 1999 bridges. Table 2 provides mix and temperature information about these experiments.

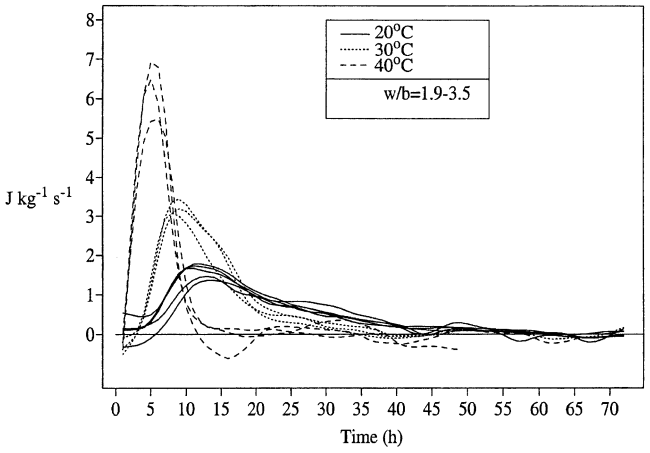

Fig. 6. Heat evolution rates from the excess water experiments (J kg^{-1} s^{-1}) with the 1999 binder samples. Information about the experiments is given in Table 3.

will use the set delay of 8 h for the 1999 bridge, as determined with 99d.

The reaction rate changes due to the Daratard 17 were implemented in the heat generation expression. With linear regression of the fractional difference in heat generation rates for 98e (with retarder) in comparison to 98a (no retarder) vs. time, we found that while the experiment time, t_{ex} (h), was greater than 9 h and less than or equal to 15 h (Eq. (13)):

$$\frac{dq_r}{dt} = \frac{d}{dt}q_{nr} + [(0.025t_{ex} - 0.3)\frac{d}{dt}q_{nr}] \quad (13)$$

where q_r is the heat generation (Eq. (4)) with retarder effects and q_{nr} is the heat generation with no retarder effects. After 15 h, the 98e rates are negligibly higher than those from 98a.

3.2. Excess water experiments (constant temperature calorimetry): k, E_a, A and n

For the excess water experiments with the 1999 binder samples, w/b was varied from 1.9 to 3.5, and reaction temperatures were set at 20, 30 and 40 °C (Table 3). The heat evolution rates from these experiments clearly show the temperature dependence of the reactions as the binder hydrated sooner and at a higher rate as the reaction temperature was increased (Fig. 6 and Table 3). The peak rate increased roughly by a factor of 2 for each increase in reaction temperature of 10 °C. The peak rates at 40 °C ranged from 5.7 to 7 J kg^{-1} s^{-1} in reasonable agreement with the variable temperature calorimetry results presented above (Fig. 4b, 99a–d,f–g).

While we believed that correcting the antifreeze temperature differences with the steady-state antifreeze temperature difference beyond 48 h would account for all heat transfers to or from the system (see Section 2.2), this proved not to be the case at 30 and 40 °C, temperatures much above the ambient laboratory temperatures. The effects of this heat transfer can be seen in the 24-h cumulative heat evolved (Table 3). At 40 °C, ~120 kJ kg^{-1} was liberated by 24 h, while the variable temperature Experiment 99c (Table 2), whose average reaction temperature was 39 °C, resulted in ~240 kJ kg^{-1} by 24 h (Fig. 5b), a 50% error. If we assume $E_a = 35$ kJ mol^{-1} and $n = 1$ for Class HP binder (see below), the 24-h 20 °C heat is 95 kJ kg^{-1} (see below), and the 40 °C heat is 240 kJ kg^{-1}, then the 24-h heat generation at 30 °C would be 170 kJ kg^{-1}, suggesting that our 30 °C heat values were too low by 18–29%. Because the steady-state antifreeze temperature differences were of the same order of magnitude as the heat generation signal (e.g., E9: 0.11 vs. 0.21 °C), heat transfer overwhelmed the hydration heat signal, resulting in considerable errors in the calculated heat values at 30 and 40 °C.

Because the ambient laboratory temperature averaged about 22 °C, heat transfer during the 20 °C experiments was small. The 24-h cumulative heat values at 20 °C for w/b = 1.9 and 2.4 (95–110 kJ kg^{-1}; Table 3) are reasonable in comparison to those given by Meland [28] for a mix of 80% Type I cement and 20% flyash at 24 h of ~115 kJ kg^{-1}. For w/b = 3.5, the heat signal from the hydrating binder was smaller than for the lower w/b and was more difficult to detect, resulting in 24-h hydration heat values about 15% less than those for the smaller water-to-binder ratios.

Heat evolution rates after the peak rate from the excess water experiments can be approximated by an exponential curve to within about 10% for the 20 °C experiments. Characteristic times (τ) were about 20 h for the 20 °C

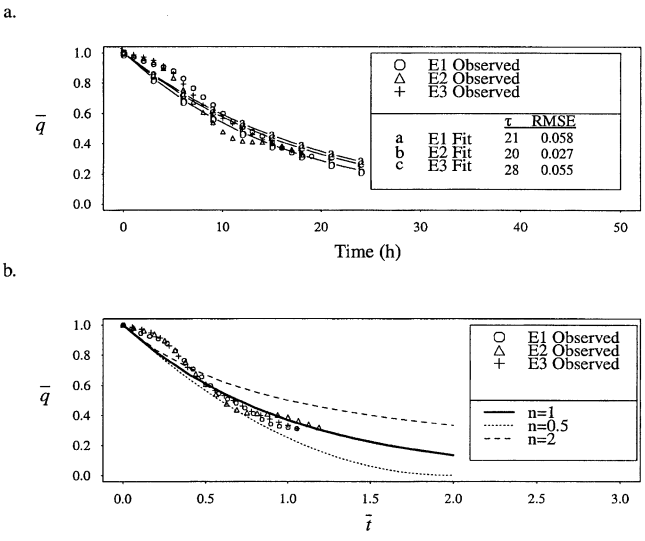

Fig. 7. (a) Time series plots of observed and fitted dimensionless heat evolution rates ($\bar{q}$, heat evolution rates scaled by the peak rate) beginning at the time of the peak rate for the 20 °C excess water experiments. The τ (h) indicated in the legend is the characteristic time of the evolution rates determined by minimizing the RMSE between the observed and exponential fitted times series. (b) Similarity plots of dimensionless heat evolution rates vs. dimensionless time ($\bar{t}$) for the 20 °C excess water experiments. Values for n indicate powers for the binder concentration in Eq. (1). See Table 3 for information on these experiments.

experiments (Fig. 7), in reasonable agreement with those obtained from the Meland [28] data (see Section 1). The assumption that $n=1$ is valid for Class HP binder.

Our excess water data gave uncertainties as small as 10% for the 20 °C results (based on the range of values at all w/b) and as large as a 65% in the 24-h heat values at 40 °C. The errors resulted in determined chemistry parameter values (n, A, k and E_a) that were either unrealistic or were uncertain (Table 4). We believe that the most appropriate analysis consists of averaging the heat data over the first 24 h ("average to end" in Table 4). Over this period, E_a ranged from 0.65 to 16.6 kJ mol^{-1}, while other published data range from 35.3 to 41.3 kJ mol^{-1} [9] and from 32.0 to 45.7 kJ mol^{-1} [24]. From our experiments, n ranged from 0.75 to 1.25, which is consistent with our arguments (Section 1 and above) that $n \sim 1$. However, since n is an exponent, small deviations from $n=1$ produce large differences in reaction rates. For example, the reaction rate (Eq. (1)) for $n=1.25$ with w/b = 1.9 is 6.8 times larger than that for $n=1$. We conclude that heat transfer during the 30 and 40 °C excess water experiments compromised the utility of the measured data in determining accurate values for A, E_a, k and n.

However, we were able to make an estimate of E_a with the 20 °C results for w/b = 1.9 (24-h heat $\sim$95 kJ kg^{-1}) and with Experiment 99a–c data, which provided an estimate of 24-h heat generation near 40 °C. Based on these data, $E_a \sim 35$ kJ mol^{-1}, in good agreement with previously published data [9,24]. Note that Kapila et al. [15] and Plawsky and Kapila [16] used $E_a = 48.0$ kJ mol^{-1}.

Since E_a was determined as a slope when heat generation rates were appropriately plotted vs. the inverse of temperature, the determined E_a is highly sensitive to the difference between the 24-h heat at 20 °C and the 40 °C values. If the 40 °C value was 10% higher than that given by 99a–c ($\sim$264 kJ kg^{-1}), $E_a = 39$ kJ mol^{-1}. If, however, the 20 °C heat was 110 kJ kg^{-1} as is seen with Experiment E3 (Table 3) and with the 99a–c values of 240 kJ kg^{-1}, $E_a = 30$ kJ mol^{-1}.

We completed our chemistry parameterization by estimating A with the 1999 variable temperature calorimetry Experiment 99c (Table 3). To do this, we modeled the simple system as discussed in Section 2.2. We focused on the temperature predictions and heat generation since these quantities were determined directly in the laboratory. We

Table 4
Parameters of the bimolecular rate expression (Eqs. (1) and (2)) determined from the excess water experiments

	Average to end
n	0.75–1.25
Order ($n+m$)	1.75–2.25
E_a (kJ mol^{-1})	0.65–16.6
A	10^{-9} to 5.5×10^{-8}
k [m^3 (mol$_R$ s)$^{-1}$]	8.0×10^{-12} to 1.3×10^{-10}

The parameters were determined with the hydration heat data averaged from the end of Stage II to the end of Stage III (average to end)

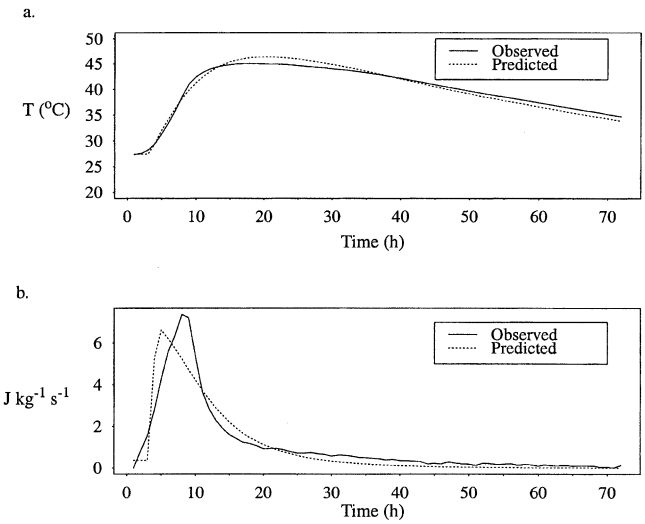

Fig. 8. (a) Time series of observed and predicted temperatures of the cement paste system in 99c (see Tables 2 and 5). (b) Time series of the observed and predicted heat generation rates of the cement paste system in 99c.

optimized the RMSE of temperature predictions by varying A in Eq. (2) systematically (we assumed $\eta \sim 7$). The value of A, which produced the lowest temperature RMSE and also gave a 72-h heat prediction within 10% of the observed value ($\sim$280 kJ kg^{-1}), was taken as the optimal value for A for these experiments. We assumed in these experiments that there was no water transport to or from the reaction chamber since it was sealed.

For 99c, the RMSE of temperature predictions was 1 °C with $A=0.0019$ and the 72-h heat generation was 260 kJ kg^{-1} (Fig. 8a). For the hydration rates (Fig. 8b), we feel that the broad representation given by our bimolecular expression provides a reasonable approximation of the observed rate.

The optimal values for A obtained for the 1999 Class HP samples ranged from 0.0016 to 0.0019 and $-\Delta H$ ranged from 260 to 268 kJ kg^{-1} (Table 5). For 99e, whose binder consisted of 100% cement, $A=0.0031$, implying a higher reaction rate in comparison to the Class HP samples, as would be expected. The RMSE of temperature predictions ranged from 0.9 to 1.4 °C. Note that temperature predic-

Table 5
Chemistry variables and model performance statistics determined from the bulk model of the 1999 variable temperature calorimetry experiments

Experiment	A (m^3 mol$_R^{-1}$ s^{-1})	RMSE T_{sys} (°C)	$-\Delta H_{sys}$ (kJ kg^{-1})
99a	0.0016	0.9	261
99b	0.0018	1.1	260
99c	0.0019	1.0	268
99d	0.0016	1.4	260
99e	0.0031	1.0	296
99f	0.0016	1.2	265

A is the pre-exponential factor of the Arrhenius expression; RMSE is the root mean squared error of the predicted system temperature (T_{sys}); and $-\Delta H_{sys}$ is the 72-h predicted hydration heat.

tions within ~2 °C of the observed were obtained with a range of A from 0.0015 to 0.0033. Because we feel our estimated heat transfer (the only boundary condition in this model) was reasonable, these RMSEs show that the bimolecular parameterization can be used to predict concrete temperatures to within ~2 °C and 72-h hydration heat within about 10%.

For binder pastes with 10% silica fume and a w/b = 0.35 (0.45), capillary pores become segmented at a hydration fraction of around 0.47 (0.66) [18], resulting in a transition from a state controlled by chemical kinetics to one controlled by the diffusion of water through the bulk material and the hydration products. Since we expect that the hydration fraction for the variable temperature calorimetry reached between 0.5 and 0.75 by 72 h [37,38], this transition most likely occurred in our samples. We do not model the concrete microstructure and so we cannot track the movement of water through the hydration products to unreacted binder. Instead, as our simulations of the hydration process proceed, the available water and binder concentrations decrease, which slows the hydration rate and the heat generation as would be expected in the mass transfer stage. Therefore, our accurate predictions of temperatures suggest that the model adequately accounts for both the chemical reaction and the mass transfer stages.

When the updated bimolecular parameterization was implemented for the 1998 bridge (A = 0.003), the RMSE of temperature predictions was about 2 °C, while those from the original Kapila et al. [15] and Plawsky and Kapila [16] formulation were 4 °C (Fig. 1). The updated hydration fraction predictions were about 0.6 by 72 h as might be expected [37,38] in comparison to 0.88 from the original predictions. We conclude that the updated bimolecular expression is an effective tool to predict concrete temperatures and hydration fractions during the first several days after the pour. Unfortunately, no observed data of the hydration fraction or available water concentrations of Class HP concrete exist for comparison with the model predictions during these early stages of hydration.

We note the overpredictions of bridge temperatures in particular following the peak temperatures (Fig. 1). This feature could be the result of inappropriate treatment of the water available for reaction (η in Eq. (3)) in the model or of the fact that during these later times, the microsilica reactions have slowed, lowering the hydration heat evolution. These possibilities are explored in greater detail in Wojcik [19].

4. Conclusions and discussion

4.1. Findings

We have improved and shown the utility of a bimolecular approach for computing heat generation rates for curing concrete at early ages (within about 3 days after the pour). We performed calorimetry experiments on samples of cement, flyash and microsilica, analyzed some published calorimetry data and implemented the approach in a model of a curing concrete bridge deck. We make the following conclusions.

(1) With the bimolecular approach, the RMSE of temperature predictions from models of our laboratory calorimetry experiments and of a curing concrete bridge deck are at most 2 °C. These simulations also resulted in 72-h heat evolution within 10% of observed values.

(2) The binder heat generation rates from the time of the peak rate until about 20 h after the peak can be approximated by an exponential function within about 15% of observed values, validating our assumption that n = 1 in Eq. (1).

(3) The total heat evolved by Class HP pastes up to 72 h, estimated from variable temperature calorimetry, was between 250 and 280 kJ kg^{-1}.

(4) By substituting 20% flyash and 6% microsilica by weight for 26% of the cement, the evolved hydration heat at 72 h was lowered by between 7% and 15%.

(5) In the 20 °C excess water experiments, the hydration reactions produced roughly 100 kJ kg^{-1} by 24 h, in good agreement with published values. Heat transfer and a comparatively weak hydration heat signal in the excess water experiments produced errors in the 24-h cumulative heat generation at 30 °C of ~25% and at 40 °C of ~50%.

(6) The activation energy for the 1999 binder components is ~35 kJ mol^{-1}.

(7) The set retarder/water reducer Daratard 17 increases the set delay and affects the hydration rates, whereas Plastiment seems only to influence the set delay. A simple parameterization is offered in which the set delay is modeled by reducing the reaction rate by a factor of 10 for a specified length of time, based on the particular admixture, admixture dosage and concrete temperature, as determined from our laboratory work and manufacturer technical data where available. The rate effects of Daratard 17 are modeled by adjusting the rate with no admixture by a time-dependent factor (ranging from 0.9 to 1.1) up to about 15 h after the peak rate.

4.2. Discussion

To develop a model to predict the thermal and moisture state of curing concrete on bridge decks to be used in a field setting, the heat generation expression used must be simple and flexible enough to allow for mix design changes at the field engineers' discretion. We have improved a bimolecular expression for the hydration process in which the cement, flyash and microsilica are lumped together as the binder components. This heat expression is similar to that from the chemoplasticity approach in that it is dependent on temperature and the degree of hydration of the binder components at a given

instance. However, our approach allows for changes in w/b, while the chemoplasticity approach does not. Charting both water and binder concentrations also allows us to predict the moisture content, degree of hydration and uniformity of hydration within a concrete mass.

In a concrete or a binder paste system, the hydration process must be seen as both a kinetic and diffusive process. In the first 2 days after mixing, especially if a sample is wet-cured, available water for reaction is abundant as the pore system of the concrete allows for the efficient uptake and transport of water as recently suggested by Bentz and Hansen [41]. After this time, the capillary pores become segmented and the hydration process increasingly is controlled by diffusion of water through the bulk material and through the hydration products. As such, for our purposes of predicting the moisture and thermal states of concrete in its early ages, it is not sufficient to consider just the kinetics or just the microstructure to adequately predict concrete temperatures. Our modeling system accounts for both aspects. In this paper, we have focused on the heat generation expression to simulate the heat released mainly during the stage dominated by the binder kinetics. We address the transport of water in concrete in Wojcik [19].

Further development of the bimolecular parameterization may include the modeling of three separate binder species (cement, microsilica and flyash) to have a better representation of the actual chemistry occurring during hydration. Because the hydration of the microsilica and flyash occurs at different time scales and under different conditions [34–36], this added detail could provide a more realistic prediction of the evolution of heat for concrete containing blended binder pastes. However, in its present form, the bimolecular expression provides a very useful approximation of the heat evolution for our stated goals.

Since the use of set retarders/water reducers is commonplace, future work must include determining the effects of these admixtures on the hydration heat evolution if accurate forecasts of concrete temperatures are to be obtained. While much is known about the general effect of the many available retarders/water reducers, we offer the first parameterization that can account for both the effects of the admixtures on set delay and the hydration rates. The utility of our parameterization can be expanded by conducting calorimetry experiments with various admixtures, admixture dosages and binder compositions.

With proper boundary conditions for the model determined from field measurement campaigns [5], this bimolecular heat expression will be used in the model to determine how atmospheric conditions during the first few critical days after pouring influence the thermal and moisture state of the concrete [19]. We will determine conditions under which a pour should and should not be allowed, information that potentially could save the NYSDOT and other similar agencies millions of dollars each year in repair costs.

Acknowledgments

We thank the New York State Department of Transportation's Research and Development Bureau, in particular former director Dr. Bob Perry, for their partial funding support of this research. Mr. Wojcik extends his thanks and appreciation to the Atmospheric Sciences Research Center (ASRC) for additional support during this project. We extend our gratitude to Dale Bentz of NIST's Building and Fire Research Laboratory for his helpful suggestions and discussions about this work. We gratefully acknowledge the assistance of Dr. Andrew J. Yencha of the University at Albany Chemistry Department with the calorimetry setup. For his skill and patience in repairing and maintaining laboratory equipment, we thank Dwayne Spiess of the Jungle Research Group at ASRC. We also thank Dr. Jim Schwab and Dr. Gar Lala of ASRC for the use of their laboratory equipment.

References

[1] A.M. Neville, Properties of Concrete, Wiley, New York, 1997.
[2] M.K. Gopalan, M.N. Haque, Effect of curing regime on the properties of fly-ash concrete, ACI Mater. J. 84 (1) (1987) 14–19.
[3] M.E. FitzGibbon, Large pours for reinforced concrete structures, Concrete 10 (3) (1976) 41.
[4] M.E. FitzGibbon, Large pours: 2, Heat generation and control, Concrete 10 (12) (1976) 33–35.
[5] G.S. Wojcik, D.R. Fitzjarrald, Energy balances of curing concrete bridge decks, J. Appl. Meteorol. 40 (11) 2003–2025.
[6] NYSDOT, The "State of the Art" Bridge Deck: Report from the Bridge Deck Task Force (1995), 58 pp. [Available from New York State Department of Transportation Structures Division, 1220 Washington Avenue, Building 5, 6th Floor, W. Averell, Harriman State Office Building Campus, Albany, NY 12232-0600].
[7] V.S. Ramachandran (Ed.), Concrete Admixtures Handbook: Properties, Science, and Technology, Noyes Publications, Park Ridge, NJ, 1984.
[8] R. Rixom, N. Mailvaganam, Chemical Admixtures for Concrete, E & FN Spon, London, 1999.
[9] D.P. Bentz, Three-dimensional computer simulation of Portland cement hydration and microstructure development, J. Am. Ceram. Soc. 80 (1997) 3–21.
[10] D.P. Bentz, Incorporation of fly ash into a 3-D cement hydration microstructure model, National Institute of Standards and Technology NISTIR 6050, US Department of Commerce, 1997.
[11] P. Acker, C. Foucrier, Y. Malier, Temperature-related mechanical effects in concrete elements and optimization of the manufacturing process, in: J.F. Young (Ed.), Properties of Concrete at Early Ages, ACI Publication, Detroit, 1986, pp. 33–47.
[12] F.-J. Ulm, O. Coussy, Strength growth as chemo-plastic hardening in early age concrete, J. Eng. Mech. (1996, December) 1123–1130.
[13] F.-J. Ulm, O. Coussy, Modeling of thermochemomechanical couplings of concrete at early ages, J. Eng. Mech. (1995, July) 785–794.
[14] F.-J. Ulm, O. Coussy, C. Hellmich, Chemoplasticity: A review of evidence, in: B. de Borst (Ed.), Computational Modeling of Concrete Structures, A&A Balkema, Rotterdam, 1998, pp. 421–439.
[15] D. Kapila, J. Falkowsky, J.L. Plawsky, Thermal effects during the curing of concrete pavements, ACI Mater. J. 94 (2) (1997) 119–128.
[16] J.L. Plawsky, D. Kapila, Cement Hydration and Heat Exchange for Curing Process of Bridge Decks at Early Stages (1997), 24 pp. [Available from New York State Department of Transportation

Research and Development Bureau, 1220 Washington Avenue, Building 7A, 7th Floor, W. Averell, Harriman State Office Building Campus, Albany, NY 12232-0600].
[17] T.C. Powers, T.L. Brownyard, Studies of physical properties of hardened Portland cement paste (nine parts), J. Am. Concr. Inst. 43 (October 1946 to April 1947).
[18] D.P. Bentz, E.J. Garboczi, Percolation of phases in a three-dimensional cement paste microstructure model, Cem. Concr. Res. 21 (1991) 325–344.
[19] G.S. Wojcik, The interaction between the atmosphere and curing concrete on bridge decks, PhD Dissertation, University at Albany, State University of New York, 2001, 280 pp.
[20] V.G. Papadakis, M.N. Fardis, C.G. Vayenas, Hydration and carbonation of pozzolanic cements, ACI Mater. J. 89 (2) (1992) 119–130.
[21] H.F.W. Taylor, Cement Chemistry, Thomas Telford Publishing, London, 1997.
[22] C.J. Brinker, G.W. Scherer, Sol–Gel Science: The Physics and Chemistry of Sol–Gel Processing, Academic Press, New York, 1990.
[23] R.K. Iler, The Colloid Chemistry of Silica and Silicates, Cornell Univ. Press, Ithaca, 1955.
[24] H. Kada-Benameur, E. Wirquin, B. Duthoit, Determination of apparent activation energy of concrete by isothermal calorimetry, Cem. Concr. Res. 30 (2000) 301–305.
[25] J. Byfors, Plain concrete at early ages, Report of the Swedish Cement Concrete Research Institute, Stockholm, 1980.
[26] D.P. Bentz, CEMHYD3D: A Three-Dimensional Cement Hydration and Microstructure Development Modelling Package, Version 2.0, US Department of Commerce, 2000 (NISTIR 6485, April).
[27] V. Baroghel-Bouny, Texture and Moisture Properties of Ordinary and High-Performance Cementitious Materials, in: Proceedings of the International Conference: Concrete: From Material to Structure, 1998, pp. 144–165.
[28] I. Meland, Influence of condensed silica fume and fly ash on the heat evolution in cement pastes, in: V.M. Malhotra (Ed.), Fly Ash, Silica Fume, Slag and Other Mineral By-Products in Concrete, vol. II, ACI Publication, Detroit, MI, 1983, pp. 665–676 (SP-79).
[29] O.M. Jensen, The Pozzolanic Reactions of Silica Fume, Building Materials Laboratory, Technical University of Denmark, Lyngby, Denmark, 1990 (in Danish; TR 229/90).
[30] D.P. Bentz, V. Waller, F. de Larrard, Prediction of adiabatic temperature rise in conventional and high-performance concretes using a 3-D microstructural model, Cem. Concr. Res. 28 (2) (1998) 285–297.
[31] D.M. Roy, The effect of blast furnace slag and related materials on the hydration and durability on concrete, Durability of Concrete — G.M. Idorn Int. Symp., ACI Publication, Detroit, 1994, pp. 195–208 (SP-131).
[32] A.L.A. Fraay, J.M. Bijen, Y.M. de Haan, The reaction of fly ash in concrete: A critical examination, Cem. Concr. Res. 19 (2) (1989) 235–246.
[33] V. Waller, F. de Larrard, P. Roussel, Modeling the temperature rise in massive HPC structures, 4th Int. Symp. on the Utilization of High-Strength/High Performance Concrete, RILEM (1996) 415–421 (May).
[34] D.M. Roy, Hydration of Blended Cements Containing Slag, Fly Ash, or Silica Fume, Proceedings of Meeting Institution of Concrete Technology, Coventry, UK, 1987, 29 pp.
[35] A.M. Alshamsi, Microsilica and ground granulated blast furnace slag effects on hydration temperature, Cem. Concr. Res. 27 (12) (1997) 1851–1859.
[36] M.I. Sánchez de Rojas, M. Frías, The pozzolanic activity of different materials, its influence on the hydration heat in mortars, Cem. Concr. Res. 26 (2) (1996) 203–213.
[37] R.H. Bogue, Chemistry of Portland Cement, Van Nostrand-Reinhold, New York, 1955.
[38] G.J. Verbeck, C.W. Foster, Longtime study of cement performance in concrete, Chapter 6: The heats of hydration of the cements, Proc. ASTM 50 (1950) 1235–1257.
[39] H.S. Fogler, Elements of Chemical Reaction Engineering, Prentice-Hall, Edgewood Cliffs, NJ, 1992.
[40] Bureau of Reclamation, Concrete Manual, US Department of the Interior, Washington, 1988.
[41] D.P. Bentz, K.K. Hansen, Preliminary observations of water movement in cement pastes during curing using X-ray absorption, Cem. Concr. Res. 30 (2000) 1157–1168.